The Astrophysical Journal, 747:31 (14pp), 2012 March 1 doi:10.1088/0004-637X/747/1/31

HOT AND COLD GALACTIC GAS IN THE NGC 2563 GALAXY GROUP

Jesper Rasmussen[1], Xue-Ning Bai[2], John S. Mulchaey[3], J. H. van Gorkom[4], Tesla E. Jeltema[5], Ann I. Zabludoff[6], Eric Wilcots[7], Paul Martini[8], Duane Lee[4], and Timothy P. Roberts[9]
[1] Dark Cosmology Centre, Niels Bohr Institute, University of Copenhagen, Juliane Maries Vej 30, DK-2100 Copenhagen, Denmark; jr@dark-cosmology.dk
[2] Department of Astrophysical Sciences, Peyton Hall, Princeton University, NJ 08544, USA
[3] Carnegie Observatories, 813 Santa Barbara Street, Pasadena, CA 91101, USA
[4] Department of Astronomy, Columbia University, Mail Code 5246, 550 West 120th Street, New York, NY 10027, USA
[5] UCO/Lick Observatories, 1156 High Street, Santa Cruz, CA 95064, USA
[6] Steward Observatory, University of Arizona, 933 North Cherry Avenue, Tucson, AZ 85721, USA
[7] Department of Astronomy, University of Wisconsin-Madison, 475 N. Charter St., Madison, WI 53706, USA
[8] Department of Astronomy, 4055 McPherson Laboratory, Ohio State University, 140 West 18th Avenue, Columbus, OH, USA
[9] Department of Physics, Durham University, South Road, Durham DH1 3LE, UK
Received 2011 May 24; accepted 2011 December 27; published 2012 February 13

ABSTRACT

The role of environmentally induced gas stripping in driving galaxy evolution in groups remains poorly understood. Here we present extensive *Chandra* and Very Large Array mosaic observations of the hot and cold interstellar medium within the members of the nearby, X-ray bright NGC 2563 group, a prime target for studies of the role of gas stripping and interactions in relatively small host halos. Our observations cover nearly all group members within a projected radius of 1.15 Mpc ($\sim$1.4 $R_{\rm vir}$) of the group center, down to a limiting X-ray luminosity and H I mass of 3×10^{39} erg s^{-1} and 2×10^{8} $M_{\odot}$, respectively. The X-ray data are consistent with efficient ram pressure stripping of the hot gas halos of early-type galaxies near the group core, but no X-ray tails are seen and the limited statistics preclude strong conclusions. The H I results suggest moderate H I mass loss from the group members when compared to similar field galaxies. Six of the 20 H I-detected group members show H I evidence of ongoing interactions with other galaxies or with the intragroup medium. Suggestive evidence is further seen for galaxies with close neighbors in position–velocity space to show relatively low H I content, consistent with tidal removal of H I. The results thus indicate removal of both hot and cold gas from the group members via a combination of ram pressure stripping and tidal interactions. We also find that 16 of the 20 H I detections occur on one side of the group, reflecting an unusual morphological segregation whose origin remains unclear.

Key words: galaxies: clusters: general – galaxies: halos – galaxies: ISM – radio lines: ISM – X-rays: galaxies

1. INTRODUCTION

Understanding the physical processes involved in the evolution of galaxies is a key goal of extragalactic astronomy. Although stellar (or halo) mass is emerging as playing a fundamental role for galaxy evolution, environmental influences may also have an impact (Kauffmann et al. 2003b, 2004; Baldry et al. 2006; Cucciati et al. 2010; Peng et al. 2010). This is particularly relevant in dense environments in which galaxies may experience a wide range of externally driven processes such as mergers, tidal interactions, and gas stripping due to interactions with ambient gas. All of these processes may act to remove a substantial fraction of the interstellar medium (ISM), or rapidly consume or eject it through interaction-induced star formation and nuclear activity, eventually leading the galaxy to transition from blue and star-forming to red and quiescent (Mihos & Hernquist 1996; Quilis et al. 2000; Verdes-Montenegro et al. 2001; Chung et al. 2007; Kawata & Mulchaey 2008).

The relative importance of these various processes should itself be a function of environment, with mergers and tidal interactions dominating in small galaxy groups (e.g., Barnes 1989; Mamon 2007), and with galaxy harassment, ram pressure stripping, and starvation (the cutoff of the supply of cold gas for star formation from warm/hot gas in the halo) becoming more efficient in massive clusters exhibiting high galaxy velocities (Moore et al. 1999; Quilis et al. 2000). *Chandra* observations do show that a lower fraction of early-type galaxies in clusters contain hot halos than their counterparts in groups (Jeltema et al. 2008), consistent with expectations of the hot halo stripping efficiency being higher in more massive systems. Evidence for ram pressure stripping of the *cold* ISM component in rich clusters is also well established through many H I studies (Chamaraux et al. 1980; Cayatte et al. 1994; Schröder et al. 2001; Solanes et al. 2001; Chung et al. 2007; Levy et al. 2007; Chung et al. 2009; Cortese et al. 2011), suggesting that interactions between galaxies and the intracluster medium may generally be an important route to removing galactic gas in the most massive systems.

The situation is less clear in smaller groups, despite these representing much more typical galaxy environments. Naively, galaxy–galaxy interactions and mergers should be relatively more important, given the lower galaxy velocities and intergalactic medium densities in groups. Indeed, the results of Jeltema et al. (2008) and Mulchaey & Jeltema (2010) show that hot X-ray halos are retained around the majority of $L_K > L^*$ early types in the central regions of groups, and these halos are not strongly X-ray underluminous compared to those of field galaxies. Hence, removal of hot halo gas by ram pressure must be very modest in groups, at least for massive galaxies. Nevertheless, numerical simulations suggest that starvation may still occur for moderate-luminosity galaxies on their first passage through even fairly small groups (Kawata & Mulchaey 2008). Viscous stripping of galactic gas through Kelvin–Helmholtz instabilities, the efficiency of which depends only linearly on galaxy velocity (Nulsen 1982), could also play a role in groups even when brute-force ram pressure is unimportant (Rasmussen et al. 2008).

For the cold gas, a number of group galaxies show evidence for extended H I that has been stripped from their host (e.g., Verdes-Montenegro et al. 2001; Kantharia et al. 2005; Kilborn

et al. 2006), and many are deficient in H I compared to similar field galaxies (Verdes-Montenegro et al. 2001; Sengupta et al. 2007; Kilborn et al. 2009). Some of these objects represent strong candidates for ram pressure stripping of both cold and hot ISM (Bureau & Carignan 2002; Rasmussen et al. 2006; Sengupta et al. 2007; McConnachie et al. 2007; Bailin & Ford 2007). However, the H I properties of spirals in these environments can often be equally well explained by tidal encounters (Kern et al. 2008; Rasmussen et al. 2008; Kilborn et al. 2009), and so it is still not fully clear which process, if any, dominates the gas removal from typical group galaxies.

Quantifying the importance of the various mechanisms acting on group galaxies requires detailed observations of the ISM in these galaxies, both within individual groups and across systems displaying a range of global properties. To identify signatures of ongoing gas removal and how these may depend on local group environment, the ISM must be probed on spatial scales of individual galaxies across the full system, with a sensitivity extending down to moderate-luminosity galaxies. Exploring the role of hot gas stripping, whether induced by ram pressure or galaxy–galaxy interactions, is currently largely limited to early-type galaxies or starbursting spirals, however, since only these galaxy types generally contain X-ray-detectable halo gas (Rasmussen et al. 2009). In more quiescent late-type spirals, gas stripping can be far more efficiently explored using H I data. Combining X-ray and H I data therefore allows one to study the ISM over the full galaxy morphological range.

Here we combine X-ray mosaicking observations from *Chandra* with analogous H I observations from the Very Large Array[10] (VLA) to study the hot and cold ISM in the nearby, X-ray bright NGC 2563 group. Our goal is to search for evidence of ongoing or recent gas stripping (we here use this term to mean any externally induced removal of gas from galaxies, including via tidal stripping), explore possible mechanisms involved, and understand their environmental dependence. While X-ray (Fabbiano et al. 1992; Mulchaey & Zabludoff 1998; Osmond & Ponman 2004; Gastaldello et al. 2007) and optical (Zabludoff & Mulchaey 1998a, 2000) observations of this group already exist, a unique aspect of the present study is that both our X-ray and H I observations cover the entire group (out to a projected radius of $R = 1.15$ Mpc, well beyond the estimated virial radius), while still benefiting from the sub-kpc spatial resolution of *Chandra* at the target redshift. Combined with the sensitivity of the VLA to low surface brightness diffuse H I emission (with a synthesized beam width of $\approx 45''$ in the most compact "D-array" configuration employed here), this enables a detailed investigation of the spatial variation in global ISM properties across the full group environment.

We describe the overall properties of the group in Section 2. The X-ray and H I analyses are detailed in Section 3, and results are presented in Section 4. Section 5 considers the evidence for recent and past ISM stripping in the group, and our results and conclusions are summarized in Section 6. We assume $H_0 = 70$ km s^{-1} Mpc^{-1}, $\Omega_m = 0.27$, and $\Omega_\Lambda = 0.73$. The target redshift of $z = 0.0157$ then corresponds to a luminosity distance of 68.1 Mpc, and $1'$ on the sky to a projected distance of 19.2 kpc. Uncertainties are quoted at the 1σ level unless otherwise specified.

[10] The Very Large Array is operated by the National Radio Astronomy Observatory, which is a facility of the National Science Foundation (NSF), operated under cooperative agreement by Associated Universities, Inc.

2. GROUP MEMBERSHIP AND PROPERTIES

Extensive optical spectroscopy of the NGC 2563 field exists from the studies of Zabludoff & Mulchaey (1998a, 2000). The field is also covered by the Sloan Digital Sky Survey (SDSS), providing images and magnitudes for all group members, and flux-calibrated spectra for most of them. From the measured redshifts, we determined group membership using the ROSTAT package (Beers et al. 1990), considering all galaxies with known recessional velocities within ± 3000 km s^{-1} of the group mean. We then calculated the biweight estimators of velocity mean and dispersion. Objects with velocities beyond $\pm 3\sigma_{\rm biwt}$ from the mean were discarded, and the process repeated iteratively until convergence. This technique identified 64 group members within a projected radius of $R = 60'$ ($R = 1.15$ Mpc) from the group center, including two newly discovered members from our H I observations (see Section 4.2). The resulting mean redshift and radial velocity dispersion of the group based on these 64 galaxies are $z = 0.0157 \pm 0.0001$ and $\sigma_{\rm biwt} = 364^{+36}_{-33}$ km s^{-1}, respectively. Based on objects classified as galaxies in the SDSS survey, the group membership is 100% (98%) spectroscopically complete down to $M_r = -18$ (-17) within $60'$ of the group center.

Group members were morphologically classified independently by J.S.M. and A.I.Z. using SDSS r-band images. The two authors' classifications agreed within one Hubble type in all cases, and our adopted morphologies represent the average of the two results. We use SDSS g-band magnitudes as a measure of the blue luminosity, and, for comparison to previous studies, K_s magnitudes from the Two Micron All Sky Survey as a rough estimate of galaxy stellar mass. The latter magnitudes are available for most of the group members, except for a few galaxies in close pairs. In these cases, the K_s magnitude was estimated from the SDSS r-band magnitude using $r - K_s = 2.90$ for early-type galaxies, and $r - K_s = 2.30$ for late types, based on the average values for the group members with both magnitudes available. The scatter in each case is $\sim$0.20. As none of the galaxies without K_s magnitudes is detected in X-rays or H I, adopting these relationships has minimal impact on our conclusions. Magnitudes were converted to solar luminosities assuming $g_\odot = 5.12$ and $K_\odot = 3.39$ after correcting for Galactic extinction. We further adopt $L^*_g = 10^{10.17}\,L_\odot$ (Montero-Dorta & Prada 2009) and $L^*_K = 10^{11.08}\,L_\odot$ (Sun et al. 2007).

While a detailed X-ray mass analysis of the group is beyond the scope of this paper, having a rough estimate of the group virial radius $R_{\rm vir}$ is instructive for the discussion to follow. This can be obtained from the hot gas temperature of $kT \approx 1.1$ keV derived by Mulchaey et al. (2003), combined with the scaling relation of Finoguenov et al. (2007). This would suggest $R_{500} \sim 420$ kpc, and hence $R_{\rm vir} \approx R_{100} \approx 2R_{500} \approx 850$ kpc in the adopted cosmology, assuming a Navarro–Frenk–White potential (Navarro et al. 1997) with a typical concentration parameter of $c = 5$–10. Here R_Δ is the radius enclosing a mean density of Δ times the critical value.

3. OBSERVATIONS AND ANALYSIS

3.1. Chandra Imaging and Spectroscopy

The distribution of group members in NGC 2563 allows most of them to be observed with 14 ACIS-I pointings: a 3×3 central mosaic to cover the inner $45' \times 45'$ of the group and five outer pointings. A total of 54 of the 64 confirmed group members were observed by *Chandra*. The majority of the remaining galaxies are optically faint and therefore not likely to be strong X-ray

Table 1
Group Members Detected with *Chandra*

Galaxy	Morphology	R (kpc)	$\log L_K$ ($L_\odot$)	$\log L_g$ ($L_\odot$)	Counts	$L_{X,th}$	$L_{X,pl}$	kT (keV)	Γ	HR	Spectrum	Notes
(1)	(2)	(3)	(4)	(5)	(6)	(7)	(8)	(9)	(10)	(11)	(12)	(13)
NGC 2563	E	0	11.43	10.54	1547	$74.2^{+5.0}_{-4.8}$	$22.6^{+5.6}_{-5.7}$	$0.97^{+0.03}_{-0.04}$	$2.16^{+0.21}_{-0.24}$	0.11 ± 0.01	1, TP	E
NGC 2562	S0/a	91	11.21	10.35	50	<1.87	$2.51^{+0.58}_{-0.45}$	0.7*	$1.84^{+0.35}_{-0.30}$	0.56 ± 0.17	2, P	E
NGC 2560	S0/a	218	11.11	10.21	139	<4.49	$8.45^{+1.65}_{-1.56}$	0.7*	$1.38^{+0.29}_{-0.27}$	0.59 ± 0.10	2, P	E
CGCG119-069	E	238	10.13	9.49	9	<5.06	<1.39	0.7*	1.7*	0.63 ± 0.42	3, U	P?
UGC 04344	Sc	238	10.14	9.91	17	<2.07	<1.86	0.7*	1.7*	0.38 ± 0.21	3, U	E?, SF
UGC 04332	Sapec	264	10.94	10.03	117	<3.82	$6.45^{+1.18}_{-1.06}$	0.7*	$1.85^{+0.27}_{-0.27}$	1.32 ± 0.25	2, P	E, Sy2
NGC 2569	E	307	10.71	9.99	18	<1.99	<2.09	0.7*	1.7*	0.26 ± 0.15	3, UT	E?
UGC 04329	Scpec	439	10.72	10.06	57	<4.03	$5.93^{+1.92}_{-1.46}$	0.7*	$2.39^{+1.16}_{-0.68}$	0.62 ± 0.17	2, P	E, SF
IC 2293	SBbc	470	10.37	9.89	9	<1.29	<1.00	0.7*	1.7*	0.20 ± 0.18	3, UT	P?, SF
2MJ082236	S0/a	542	9.99	9.32	13	<1.57	<1.53	0.7*	1.7*	0.49 ± 0.28	3, U	E?, SF
NGC 2557	SB0	567	11.15	10.29	162	$11.2^{+3.0}_{-2.3}$	$10.4^{+1.4}_{-1.2}$	$0.34^{+0.10}_{-0.07}$	1.7*	0.27 ± 0.05	1, TP	E, LI
UGC 04324	Sab	664	10.71	9.92	35	<3.63	<3.96	0.7*	1.7*	0.42 ± 0.16	3, U	E, SF
NGC 2558	Sb	739	11.03	10.26	45	<2.45	$3.90^{+0.86}_{-0.75}$	0.7*	$1.53^{+0.30}_{-0.33}$	0.45 ± 0.15	2, P	E, LI
IC 2338	SBcd	848	10.27	9.87	59	<3.09	$4.75^{+1.02}_{-0.95}$	0.7*	1.7*	0.35 ± 0.10	2, TP	E, SF
IC 2339	SBcpec	858	10.48	10.02	32	$1.85^{+0.91}_{-0.84}$	$1.69^{+0.67}_{-0.60}$	0.7*	1.7*	0.21 ± 0.10	1, TP	E, SF
CGCG119-047	Sab	923	10.62	10.04	26	<2.80	<2.68	0.7*	1.7*	0.36 ± 0.16	3, U	P?, SF
IC 2341	E/S0	929	10.91	10.19	32	<3.54	<2.89	0.7*	1.7*	0.88 ± 0.31	3, U	E, LI

Notes. Column 3: projected distance from peak of the intragroup X-ray emission. Column 6: net counts in the "full" 0.3–7 keV band. Column 7: 0.5–2 keV thermal luminosities (10^{39} erg s^{-1}). Column 8: 0.5–2 keV power-law luminosities (10^{39} erg s^{-1}). Column 9: best-fit X-ray temperature; asterisk indicates a fixed value. Column 10: best-fit power-law index; asterisk indicates a fixed value. Column 11: (2–7 keV)/(0.3–2 keV) hardness ratio. Column 12: classification of the X-ray spectrum according to statistical quality (1–3, as described in Section 3.1), and according to consistency with a power law only (P), both thermal and power-law components present (TP), or spectral composition unknown (U), but hardness ratio suggests thermal component present (T). Column 13: specification of whether the X-ray emission is extended (E), point-like (P), or uncertain ("?"), and whether the galaxy is star-forming (SF), a LINER (LI), or Seyfert II (Sy2).

sources. The 14 pointings were done between 2007 June and 2008 March for 30 ks each, except for the central pointing which was observed for 50 ks to achieve a similar contrast for galaxies in the X-ray bright central region. All observations were conducted in VFAINT telemetry mode. The level 1 event files were processed with CIAO[11] v4.0 and CALDB[12] v3.4.3, filtering out bad pixels and applying the latest gain files. Events with *ASCA* grades[13] 1, 5, and 7, and a non-zero status flag were discarded. Finally, background flares were screened for using the routine "lc_clean.sl" in CIAO, excluding time periods with background count rates greater than 20% of the quiescent rate. Flaring was not a problem for any of our observations.

Source detection was performed using the "Mexican Hat" wavelet source detection algorithm "wavdetect" in CIAO, with scales of 1, 2, 4, 8, 16, and 32 pixels, using soft (0.3–2.0 keV), hard (2.0–7.0 keV), and "full" band (0.3–7 keV) event lists. The detection threshold was set to limit the number of false detections to ≈4 per CCD. As summarized in Table 1, a total of 17 confirmed group members were detected, including the largest elliptical, NGC 2563 itself. This galaxy is coincident with the group center as defined by the peak of the diffuse group X-ray emission. As it is not straightforward to cleanly separate the emission of this galaxy from that of the intragroup medium, the central galaxy is treated as a special case for the remainder of the paper.

For all detected group members, source spectra and associated response files were extracted within circular regions extending to where the galaxy surface brightness becomes consistent with the local background level. Background spectra were extracted in surrounding annuli, and results were fitted in the 0.3–7.0 keV band using XSPEC v. 12.3 (Arnaud 1996). As many of the sources have few counts, the maximum likelihood-based C-statistic (Cash 1979) was used to determine best-fit parameters. The goodness of fit was verified using the χ^2 statistic for all sources with sufficient photon statistics to allow meaningful constraints from spectra accumulated in bins of at least 20 net counts.

The X-ray emission in luminous early types is generally dominated by that of hot gas and low-mass X-ray binaries (e.g., Fabbiano 2006). We modeled any hot gas emission in the group members using the *mekal* optically thin thermal plasma model (Mewe et al. 1985; Liedahl et al. 1995) in XSPEC, assuming solar abundance ratios. Any X-ray binary/active galactic nucleus (AGN) component was modeled with a power law. In all fits, the absorbing hydrogen column density was fixed at the Galactic value ($N_H = 4.0 \times 10^{20}$ cm^{-2}; Kalberla et al. 2005), since the limited photon statistics generally precluded useful constraints on N_H from spectral fitting itself. Following Sun et al. (2007) and Jeltema et al. (2008), the metallicity in the *mekal* model was fixed at 0.8 $Z_\odot$, the mean value found for galactic hot gas in the large cluster galaxy sample of Sun et al. (2007). This left four free model parameters: Gas temperature T, power-law index Γ, and two normalizations. However, due to limited number of counts, the 3σ uncertainties on T and Γ were unconstrained for most of the galaxies. In such cases we first fixed Γ at 1.7, as is typical for X-ray binary and AGN spectra, and, if necessary, also T at 0.7 keV. Based on the photon statistics and spectral results, the detected galaxies were then divided into three categories, as summarized in Column 12 of Table 1.

1. Galaxies for which the normalization of both components was well constrained at the 2σ level (three galaxies in total;

[11] http://cxc.harvard.edu/ciao/
[12] http://cxc.harvard.edu/caldb/
[13] See http://cxc.harvard.edu/ciao/ahelp/acis_process_events.html

well constrained here means that the 2σ uncertainties are finite, and that the normalization is non-zero within those uncertainties). For the central galaxy NGC 2563, all of the four parameters are well constrained, but its emission is not easily deblended from that of the intragroup medium. The other two galaxies are NGC 2557, where Γ was fixed, and IC 2339, where also T was fixed. Best-fit values and 1σ errors for all fit parameters were determined using Markov Chain Monte Carlo (MCMC) simulations in XSPEC. The values reported were obtained from the median value of the chain. We note for completeness that the standard deviation leading to a parameter being here considered well constrained (which is based on the change in the adopted fit statistic when the parameter is varied, using XSPEC's standard "error" command) is not necessarily identical to that resulting from the MCMC simulations.

2. Galaxies with $\gtrsim$30 counts but for which the normalization of one or both components remained unconstrained within the 2σ uncertainties (six galaxies in total). In the cases where the 2σ lower limit on the thermal luminosity $L_{\rm X,th}$ was consistent with zero, whereas that on the power-law component was not, the spectrum was assumed to be consistent with a power law only. IC 2338 is consistent with displaying both a thermal and a power-law component, but, unlike galaxies in category (1), its 2σ upper limit on $L_{\rm X,th}$ remained unconstrained. Using MCMC, we report the corresponding 1σ upper limit. For the remaining galaxies in this category, the best-fit Γ was consistent with $\approx$1.7 as expected from X-ray binaries or an AGN, whereas the best-fit temperature was much higher ($T > 4$ keV) than expected for hot galactic gas. Hence, a power-law component likely dominates their X-ray output. For these sources, we fixed the best-fit power-law model and added a $T = 0.7$ keV thermal component. The limit on $L_{\rm X,th}$ was determined from the 1σ upper limit of the normalization of the *mekal* model.
3. Galaxies detected with $\lesssim$30 net counts (eight in total). In these cases, statistics are insufficient to allow a robust determination of the nature of their X-ray emission. A 1σ upper limit to their $L_{\rm X,th}$ was estimated assuming a $T = 0.7$ keV *mekal* model, but these galaxies are labeled with "U" (for unknown spectral composition) in Column 12 of Table 1. To help clarify the nature of these sources, we also considered their hardness ratios HR (here the 2–7 keV/0.3–2 keV flux ratio). This ratio is 0.02–0.05 for a *mekal* model with $T = 0.7$–1.0 keV, and 0.35–0.47 for a power-law spectrum with $\Gamma = 1.7$–2.0. For $0.05 < {\rm HR} < 0.35$, the dominant component is ambiguous, but some contribution from a thermal component is allowed. Although these classifications are only tentative, given the Poisson uncertainties on HR, we do note that all group members spectroscopically confirmed to require only a power law show ${\rm HR} > 0.4$, whereas ${\rm HR} \lesssim 0.35$ for the galaxies with a spectroscopically identified thermal component. In Table 1, a "T" is listed after "U" in Column 12 if ${\rm HR} < 0.35$ to indicate that the galaxy may contain thermal emission. The remaining galaxies are labeled with either "TP," meaning that both thermal and power-law components are likely present ($0.05 < {\rm HR} < 0.35$), or "P," indicating consistency with a power law only (${\rm HR} > 0.35$).

To further aid in identifying the nature of galactic X-ray emission, we used its spatial extent to help discriminate between nuclear (AGN) and galaxy-wide emission (e.g., hot gas halos, X-ray binaries). For each detected group member, we fitted the 0.5–2 keV brightness profile with a Gaussian, and classified it as extended if the 1σ lower bound of its full width at half-maximum (FWHM) was $\geqslant$ 10% larger than that of the local point-spread function (PSF) extracted at peak source energy. Overall, most of the detected group members appear extended in X-rays, and these are labeled with an "E" in Column 13 of Table 1, or with a "P" (point-like) otherwise. For most sources with $\lesssim$30 counts the extent remains poorly constrained, however, and Column 13 then includes a question mark.

For the X-ray-undetected group members, we followed the procedure of Sun et al. (2007) and Jeltema et al. (2008) to estimate luminosity upper limits. Count rates were measured within a circular aperture of $R = 3$ kpc from the optical galaxy center, in a few cases expanded to include the 90% encircled energy radius of the local PSF at $E = 1$ keV to account for PSF smearing. The upper limit on $L_{\rm X,th}$ was derived from the Poisson 3σ upper limit on the count rate (Gehrels 1986) assuming a $T = 0.7$ keV *mekal* model.

3.2. VLA Observations and Analysis

The H I analysis was based on two different observing runs at the VLA in its most compact, 1 km (D-array), configuration. The first run, done in 1999, covered the entire group with a 6×6 point mosaic. Individual pointings were separated by 15′, fully sampling the primary beam with its FWHM of 30′. To probe as wide a velocity range as possible with sufficient velocity resolution, we used a total bandwidth of 3.125 MHz and four intermediate frequency (IF) channels with two frequency settings and slightly overlapping bands. The total velocity range covered was $\sim$1100 km s^{-1} with a resolution of 20 km s^{-1}. The data were calibrated using standard AIPS[14] procedures, and then imported into MIRIAD[15] for mosaicking and joint deconvolution, turning the individual pointings into one mosaicked cube for each IF. The continuum was then subtracted from the u–v data using a fit through the line-free channels identified within the cube. However, inspection of the final cube showed that our velocity coverage was insufficient, with several group members detected close to the edge of the band and their H I velocity range only partly probed.

To remedy this, NGC 2563 was reobserved in 2007, using a 14-point mosaic that covered an area identical to that of our *Chandra* mosaic. To also cover a larger velocity range, we used a total bandwidth of 6.25 MHz with two IFs and no online Hanning smoothing. Each pointing was observed at two separate frequencies, resulting in a total velocity coverage of 2100 km s^{-1}. Each pointing and velocity setting was calibrated separately, and cubes were made using AIPS. Overlapping frequencies were then combined in the image plane, resulting in a 101-channel cube per pointing. After identifying channels containing H I, the continuum was iteratively subtracted from each cube using a linear fit in the image plane through the line-free channels. The resulting cubes were then CLEANed, combined into one, and the output corrected for the primary beam response; where cubes overlapped, they were averaged with weighting that accounted for the location within the pointing and for the distance from the center of each field. Although interference generated by the VLA rendered data unusable within a narrow velocity range (4331–4374 km s^{-1}),

[14] http://www.aips.nrao.edu/
[15] http://www.atnf.csiro.au/computing/software/miriad/

Table 2
Parameters of the VLA D-array Observations

Parameter	36-point Mosaic	14-point Mosaic
R.A. (J2000)	08 20 23.7	08 20 23.7
Decl. (J2000)	21 05 00.5	21 05 00.5
Velocity range (km s^{-1})	4364–5449	3834–5942
Velocity resolution (km s^{-1})	21	21
Synthesized beam ($''$)	70×59	64×53
rms noise (mJy $beam^{-1}$)	0.5	0.6

the only group member affected is an Sm dwarf with $L_K \approx 1 \times 10^9\ L_\odot$, so this has little impact on our results.

Instrumental parameters and specifics of the cubes for both data sets are summarized in Table 2, including their velocity ranges (heliocentric, optical definition). Since complete velocity coverage is important here, the 36-point mosaic was used exclusively to search for H I emission, combining it with the central part of the 14-point mosaic. All remaining H I analysis employed the 14-point mosaic only. This was searched for neutral hydrogen using three different methods. First, the 101-channel cube was divided into groups of 25, smoothed spatially to half resolution, and Hanning-smoothed in velocity. This was then used as a mask for the full-resolution cube, blanking all pixels below 2σ in the smoothed cube and summing over 25 channels. Next, we searched the cube by eye, stepping through the velocity channels at different speeds and comparing our detections with the first method. Finally, we plotted spectra integrated over a few beams at the location of the optically identified group members. This did not give any additional detections, so our search was essentially an optically blind one.

Figure 1 shows a gray-scale image of a typical channel in the cube to illustrate the spatial noise distribution and the position of the group members. In the central square degree ($R \lesssim 600$ kpc $\approx 0.7 R_{\rm vir}$) the rms noise (using robust weighting) is remarkably uniform at 0.6 mJy $beam^{-1}$, equivalent to $N_{\rm H} \simeq 4 \times 10^{18}$ cm^{-2}. Assuming 3σ over five channels, the corresponding sensitivity is $M_{\rm H\,I} = 2 \times 10^8\ M_\odot$. Along the $9'$ wide outer edges, the noise and sensitivity rise to 3.0 mJy $beam^{-1}$ and $1 \times 10^9\ M_\odot$, respectively, due to the correction for the primary beam response. This only affects five out of the 64 group members and none of our conclusions. A total noise-free H I image was produced by again using the smoothed cube as a mask and summing each detected galaxy over the narrow velocity range in which H I was detected. The total H I mass for each galaxy was then determined by summing the flux in individual channels in a box centered on the galaxy. The resulting typical uncertainty is 10% for the galaxies with $M_{\rm H\,I}$ above a few times $10^9\ M_\odot$, and $2 \times 10^8\ M_\odot$ for the remainder.

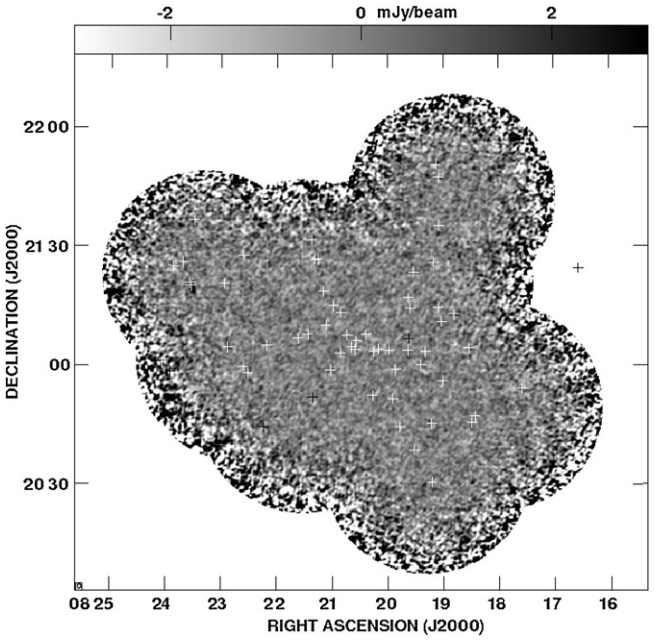

Figure 1. Gray-scale image of a typical channel in the H I data cube for the 14-point VLA mosaic. Crosses mark the position of the group members. The one group member not covered in the 14-point VLA mosaic, IC 2253, was observed but not detected in the 36-point mosaic.

4. RESULTS

4.1. X-Ray Results

Table 1 lists all 17 X-ray-detected group members (of the 54 observed), and whether these show evidence for star formation or AGN activity. This is based on their location in a BPT diagram (Baldwin et al. 1981; Kewley et al. 2001; Kauffmann et al. 2003a), as inferred from an emission-line analysis of their SDSS spectra, with optical line fluxes measured using the code described in Tremonti et al. (2004).

Figure 2 shows a 0.5–2 keV mosaic image of the group from our 14 *Chandra* pointings, adaptively smoothed using the "csmooth" algorithm, with signal significance set between 3σ–5σ. To produce this, spectrally weighted exposure maps were smoothed to the same spatial scales, and the exposure-corrected images combined into one. The impact of edge effects was reduced by removing regions with (smoothed) exposure values below 3% of the maximum, but small enhancements at the boundaries of adjacent pointings still remain. Detected group galaxies are marked with squares in the figure, with interlopers accounting for the remaining X-ray sources.

Due to the spatial variation in *Chandra* effective area, our X-ray detection limits are not uniform across the field, but we reach a 3σ upper limit in the 0.5–2.0 keV band of $L_{\rm X} \approx 3 \times 10^{39}$ erg s^{-1} or better for all of the observed group members. These span almost three orders of magnitude in L_K, with nearly all galaxies above $0.5L^*$ in the g or K band detected in X-rays (7/8 in K, 15/16 in g), whereas the corresponding fraction is less than half (4/9) for those fainter than $0.2L_K^*$. This is qualitatively consistent with other studies which show a strong correlation between galaxy optical and X-ray luminosity (Fabbiano et al. 1992; Read & Ponman 2001; O'Sullivan et al. 2001, 2003). As noted earlier, the 10 members not observed by *Chandra* are mostly optically faint, with seven below $0.1L_K^*$ and only one above L_K^*.

Among the nine galaxies for which X-ray spectral fitting provides useful constraints (cases 1 and 2 in Section 3.1), four show evidence for a thermal component, including the central NGC 2563 itself. From the hardness ratios of the remaining (case 3) galaxies, two additional objects show evidence for thermal emission for a total of six such galaxies. However, recalling from Section 3.1 that HR < 0.05 for a thermal-only model, we note that no source besides NGC 2563 itself has a hardness ratio HR < 0.2, so a power-law component is likely present (if not dominant) in all the X-ray-detected galaxies. In all group members with more than 40 counts, the emission is inferred to be spatially extended, and their smoothed 0.5–2 keV contours overlaid on SDSS r-band images are shown in Figure 3. Note the offset between the X-ray peak and the optical center

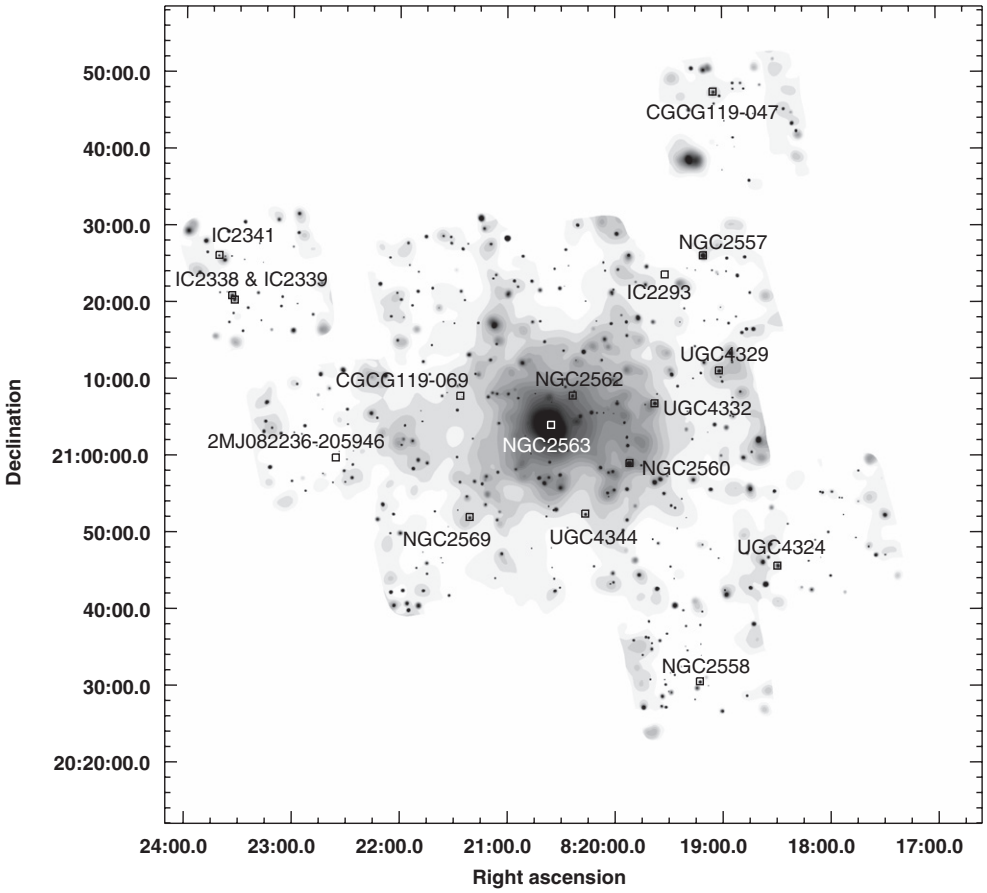

Figure 2. Adaptively smoothed 0.5–2.0 keV image of the NGC 2563 group from our 14 *Chandra* ACIS-I pointings, with intensity plotted on a log scale. All group members detected in the unsmoothed *Chandra* data are marked with squares.

in NGC 2560, possibly indicating the presence of an ultra-luminous X-ray source as seen in other nearby galaxies (Miller & Colbert 2004; Roberts 2007).

Previous studies have revealed a correlation between L_K and thermal X-ray luminosity for early-type galaxies in all environments (O'Sullivan et al. 2001; Sun et al. 2007; Jeltema et al. 2008; Mulchaey & Jeltema 2010). Taking early types to be Sa or earlier for consistency with these works, then roughly half of the members in NGC 2563 belong to this category. Figure 4(a) compares $L_{\rm X,th}$ for our optically bright group members to the scaling relation derived by Jeltema et al. (2008) for early types in groups. The central galaxy NGC 2563 itself is excluded here for reasons discussed earlier. Our two other early types with evidence for a thermal component (NGC 2557 and NGC 2569) are consistent with the Jeltema et al. (2008) relation, while the majority of the X-ray-undetected galaxies are too optically faint to offer much further insight with the present X-ray detection limits. With the limited statistics, we simply conclude that the detected early types in NGC 2563 do not deviate significantly from the L_X–L_K relation found for other group ellipticals.

To further elucidate the potential hot gas contribution to the total L_X of our early types, Figure 4(b) compares the 0.3–8 keV L_X of the X-ray-detected group members to that expected from low-mass X-ray binaries using the scaling relation of Kim & Fabbiano (2004). NGC 2563 itself is again excluded. None of our early types shows evidence of a significant X-ray excess relative to this expectation, suggesting that the majority of their X-ray output is of stellar origin. A few of the more luminous galaxies even lie below this relation, including NGC 2557 which does contain a thermal component.

Of the eight X-ray-detected late-type members, three show evidence for a thermal component. All eight galaxies have $L_g > 0.5L_g^*$ but span a relatively larger range in L_K, suggesting their total X-ray output is more directly related to the blue stellar light than to stellar mass. We note the similarity to other studies of late-type galaxies that find their diffuse L_X to correlate more strongly with L_B (and hence star formation rate) than with L_K or stellar mass (Tüllmann et al. 2006; Sun et al. 2007). Our SDSS spectra generally support this, with seven of our eight X-ray-detected late-type members showing optical line emission consistent with star formation. The eighth galaxy (NGC 2558) has line ratios consistent with a LINER. Based on the BPT diagram, there are 12 other actively star-forming late types in the group, but all have $L_g < 0.5L_g^*$ and remain X-ray undetected.

4.2. H I Results

We detect H I in 20 of the 64 group members down to our H I mass limit of $\sim 2 \times 10^8\,M_\odot$ (recall that our limits are higher for galaxies at the very edge of the VLA mosaic). The results for these 20 objects are summarized in Table 3, along with results for three large spirals that remain undetected in H I but whose H I deficiencies can still be estimated (see below). Quoted H I velocity widths correspond to the velocity range of channels with signal at the $\geqslant 2\sigma$ level; note that for UGC 04332 the H I profile extends to the edge of our velocity

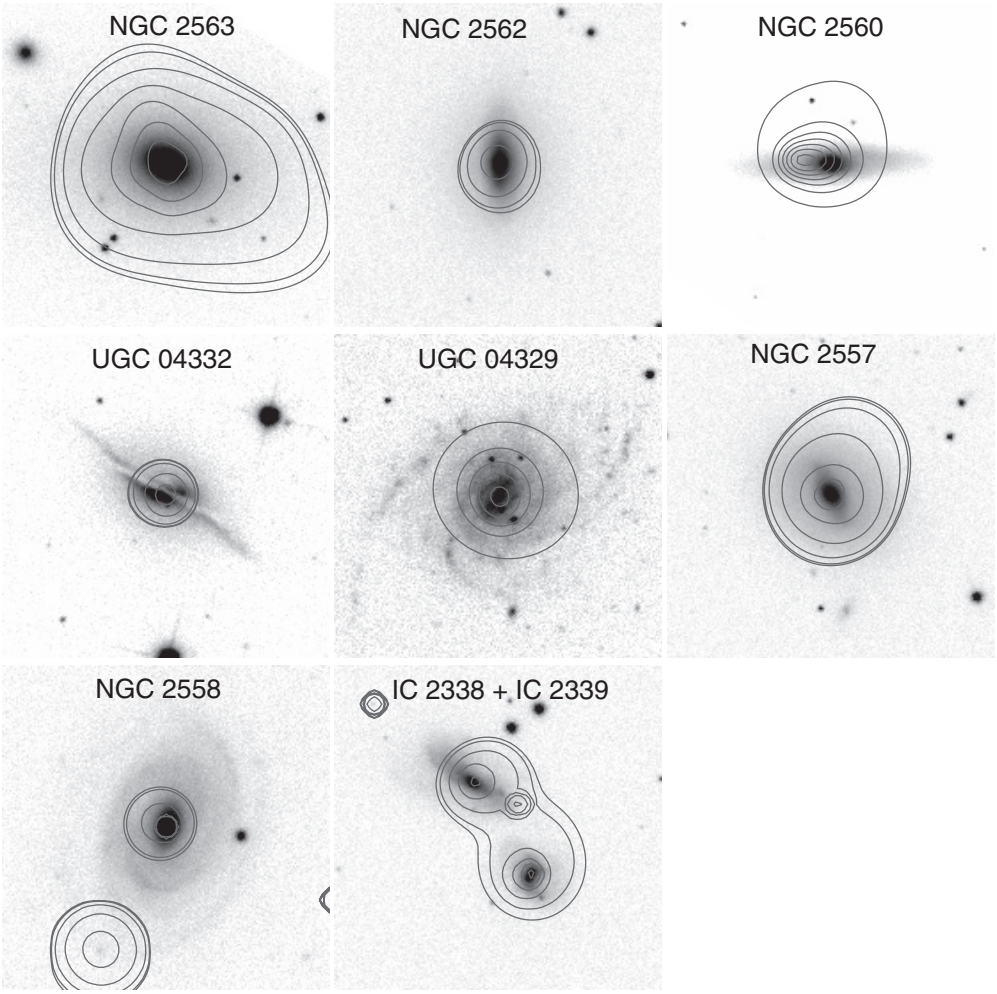

Figure 3. Smoothed 0.5–2 keV X-ray contours overlaid on SDSS *r*-band images for the eight X-ray brightest group members. Each image is $2' \times 2'$ ($\sim 40 \times 40$ kpc).

coverage, so the H I width and mass provided in Table 3 are lower limits. Two of the 20 H I detections are associated with galaxies not previously identified as group members from optical spectroscopy (SDSSJ082044.60+210715.0 and SDSSJ081931.17+203843.9). Both of these represent optically faint irregular galaxies.

H I is detected only in galaxies of types Sa and later, including in all 15 such galaxies with $L_K > 0.1L_K^*$. Figure 5 shows contours from our noise-free H I mosaic overlaid on the *Chandra* mosaic of the full group, and Figure 6 displays an H I/optical overlay for each H I-detected galaxy. The latter figure reveals four significant H I extensions in the group associated with six galaxies (IC 2238/IC 2339, UGC 04324/CGCG119-040, CGCG119-047, and CGCG119-051, all labeled with an asterisk in the figure). This implies that ~30% of our H I-detected group members display H I evidence for being involved in an ongoing interaction. The galaxies IC 2338 and IC 2339 represent a particularly close pair, and the H I quantities quoted in Table 3 therefore apply for the entire system. The absence of detectable H I among the early-type group members is consistent with previous studies finding H I above our detection limits in only a small fraction of early types (Burstein et al. 1987; Morganti et al. 2006; di Serego Alighieri et al. 2007). Since we have performed an optically blind search for H I across the entire group, we can furthermore rule out the existence of any optically dark H I clouds not associated with any galaxy down to our H I mass limit.

To investigate to what extent the group members may be deficient in H I, we estimated H I deficiencies $\mathrm{Def_{H\,I}}$ following the usual prescription,

$$\mathrm{Def_{H\,I}} = \log\left(M_{\mathrm{H\,I}}\right)_{\mathrm{expected}} - \log\left(M_{\mathrm{H\,I}}\right)_{\mathrm{observed}}. \quad (1)$$

The expected H I masses were computed from the best-fit relationship between total H I mass and galaxy optical diameter D derived for galaxies in the field (Solanes et al. 1996). D is here defined as the galaxy major axis measured from the Palomar Observatory Sky Survey blue prints; where not already available from the Uppsala General Catalog of Galaxies (Nilson 1973), we measured D directly from these prints. As the Solanes et al. (1996) field sample was restricted to rather large spirals of types Sa through Sc, only group members of those types and with $D > 10$ kpc were considered here. Note, as mentioned above, that this includes three galaxies not detected in H I, and these are also listed in Table 3. For the IC 2338/2339 pair, a single deficiency was calculated from the total observed and expected H I masses given the optical sizes of both galaxies.

The resulting deficiencies listed in Table 3 span a wide range, but given the uncertainties in D and optical morphology, as well as the dispersion in the H I masses of field galaxies, objects with observed H I masses within a factor of a few of the expected values cannot be considered deficient. However, there are six galaxies with $\mathrm{Def_{H\,I}} \gtrsim 0.45$, consistent with an H I deficiency of

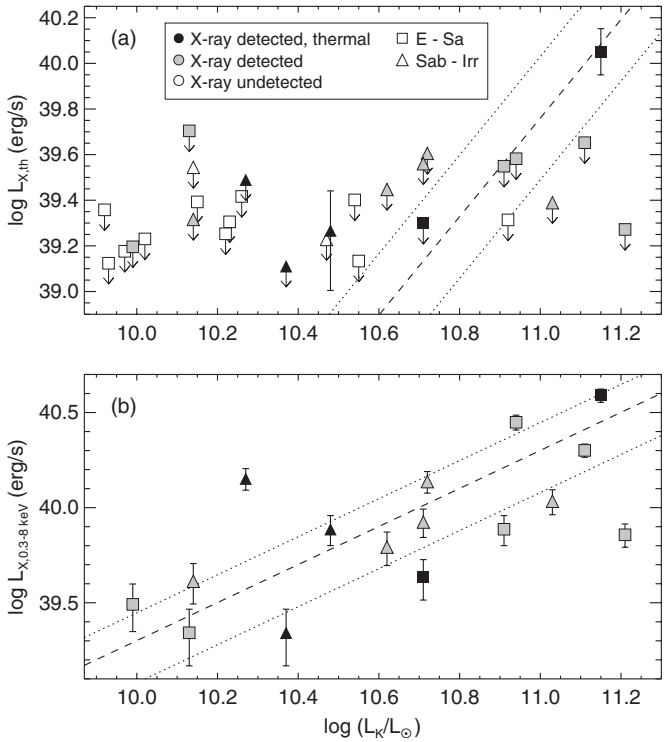

Figure 4. (a) Thermal X-ray luminosities of all optically bright group members covered by *Chandra* (excluding the central NGC 2563 itself), and the corresponding scaling with galaxy L_K for early types in groups from Jeltema et al. (2008, dashed) and its 3σ errors (dotted). Black symbols represent galaxies with evidence for a thermal component, gray symbols the remaining X-ray-detected galaxies, and empty symbols the X-ray-undetected objects. Early-type galaxies are shown by squares, late types by triangles. (b) 0.3–8 keV L_X for all X-ray-detected members, again excluding NGC 2563 itself, along with the scaling relation (and 1σ errors) for total L_X from low-mass X-ray binaries in early types from Kim & Fabbiano (2004). Symbols are as above.

at least a factor of three. One of these is UGC 04386, but $\mathrm{Def_{H\,I}}$ for this object is not well established, in part because it resides at the eastern edge of the H I mosaic where the data are noisier, and in part because it is viewed edge-on and is of uncertain morphological type.

4.3. The Intragroup Medium

Although our main goal is to study the ISM in individual group members, it is also relevant to establish which galaxies are embedded within detectable intragroup gas. To do so, a radial surface brightness profile was extracted from the unsmoothed exposure-corrected *Chandra* mosaic, centered on NGC 2563 itself, and with all other bright sources masked out. The background level was estimated from the four outermost pointings, which are all centered at $R = 40'$–$45'$ from the X-ray peak and show consistent full-chip count rates. The resulting background-subtracted profile, shown in Figure 7, reveals diffuse emission out to at least $R \approx 21'$ (≈400 kpc in projection). This is a few arcminutes further than the maximum extent determined from *ROSAT* observations (Mulchaey et al. 2003; Osmond & Ponman 2004), and roughly corresponds to our estimate of $R_{500} \approx 420$ kpc. Modeling the profile as a sum of two β-models yields $\beta_1 = 0.61^{+0.09}_{-0.03}$, $r_{c1} = 1.0 \pm 0.1$ kpc, and $\beta_2 = 0.32 \pm 0.01$, $r_{c2} = 1.1^{+1.3}_{-1.0}$ kpc for the inner and outer components, respectively. With a reduced $\chi^2 = 3.0$, the fit is poor however, in part because the profile steepens beyond that

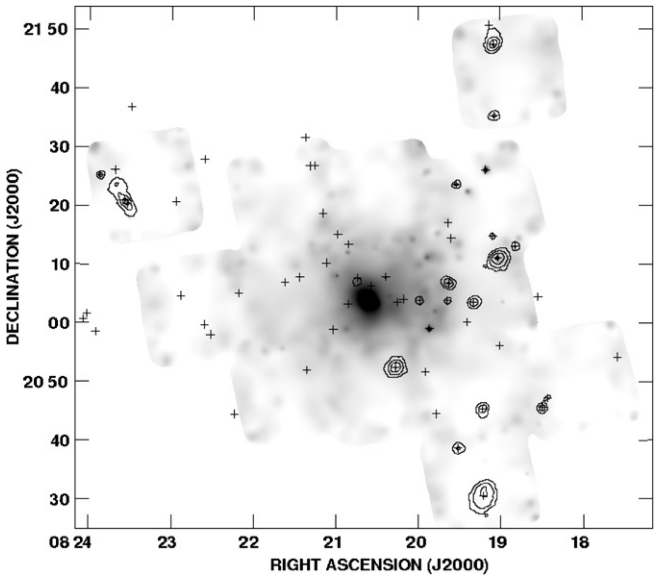

Figure 5. 0.5–2.0 keV gray-scale image of the group, with total H I contours overlaid at 0.04, 0.4, 1.2, and 2.4 Jy beam^{-1} km s^{-1} (corresponding to $N_{\mathrm{H}} = 1.27$, 12.7, 38.2, and 76.4 $\times$ 10^{19} cm^{-2}). Individual group members are marked by crosses; IC 2253, not covered by the 14-point VLA mosaic, is not included.

of a β-model at large radii, as also seen in other groups and clusters (Vikhlinin et al. 2006; Sun et al. 2009).

The relatively high central surface brightness could potentially compromise our ability to detect individual galaxies in the group core. We have attempted to circumvent this issue by requiring a longer central *Chandra* exposure (50 ks). In addition, the surface brightness has dropped from its central value by three orders of magnitude already at $R = 5' \approx 100$ kpc. Apart from the central galaxy, there are no optically luminous group members within the central few arcmin, so our X-ray detection limits are impacted minimally by the presence of intragroup gas. This is corroborated by the fact that we find no systematic radial variation in limiting $L_{\mathrm{X,th}}$ for the 54 group members covered by *Chandra*. A detailed analysis of the intragroup medium in NGC 2563 will be the subject of future work.

5. GAS STRIPPING IN NGC 2563

With our H I and X-ray results extending well beyond the group virial radius, we can now explore how the ISM properties of individual galaxies vary with position across the entire group, and in particular to what extent there is evidence for ongoing or recent ISM stripping from the group members.

5.1. Evidence for Ram Pressure Stripping

The detection of X-ray tails with *Chandra* has provided direct evidence for ram pressure stripping in both groups (Rasmussen et al. 2006; Jeltema et al. 2008) and clusters (Sun et al. 2007), and similar inferences have been made from the presence of H I tails within these systems (Kenney et al. 2004; Crowl et al. 2005; Chung et al. 2007). In X-rays, however, the detection rate of these features is generally very small (<10%), suggesting that strong stripping of hot ISM is either very rare or proceeds very rapidly. No evidence for such activity in the form of X-ray tails is seen within NGC 2563, but this is not surprising given the low detection rate of thermal coronae within the sample.

In H I, we identify two tails associated with the relatively isolated CGCG119-047 and CGCG119-051, both with H I

Table 3
H I Detections and Deficiencies

Galaxy	Morphology	R (kpc)	H I width (km s^{-1})	H I Velocity (km s^{-1})	Optical Velocity (km s^{-1})	Log ($M_{\rm H\,I}$) ($M_\odot$)	$\rm Def_{H\,I}$
SDSSJ082044.60+210715.0	Irr	73	42	4406[a]	...	8.28	...
CGCG119−061	Sab	112	...	...	5235	<8.60[b]	>+0.56
CGCG119−059	Sc	165	170	4215	4211	8.73	+0.39
UGC 04344	Sc	238	149	5033	5041	9.89	−0.10
SDSSJ081938.81+210353.0	Irr	254	43	4236	4240	8.48	...
UGC 04332	Sa pec	264	>449[c]	5481	5514	>9.41[c]	<+0.04[c]
CGCG119−053	Sa pec	339	171	4852	4877	9.26	−0.17
UGC 04329	Sc pec	439	254	4109	4099	9.98	+0.10
SDSSJ081905.46+211448.0	Sm?	451	106	4842	4844	8.51	...
IC 2293	SBbc	470	212	4088	4094	8.91	+0.55
CGCG119−043	Sc pec	506	170	4470	4458	8.65	+0.47
CGCG119−051	Sb[d]	513	191	5033	5028	9.32	−0.02
SDSSJ081931.17+203843.9	Irr	564	85	4980[a]	...	8.81	...
CGCG119−040	Sa	663	21	4841	4816	7.78	+1.23
UGC04324	Sab[d]	664	340	4831	4814	9.20	+0.32
SDSSJ081904.25+213521.0	Irr	724	106	4863	4865	8.95	...
NGC 2558	Sb	739	405	4990	4998	10.08	−0.23
IC 2338	SBcd[d]	848	313[e]	5413[e]	5400	9.76[e]	−0.34[e]
IC 2339	SBc pec	858	313[e]	5413[e]	5420	9.76[e]	−0.34[e]
CGCG119−082	SBa	898	...	...	4783	<9.00[b]	>+0.09
UGC 04386	Sab pec	921	...	...	4640	<9.00[b]	>+0.61
CGCG119−047	Sab[d]	923	276	4502	4506	9.73	−0.45
SDSSJ082352.25+212507.2	Sc	964	171	5086	5095	8.85	+0.45

Notes.
[a] New H I group member.
[b] H I undetected.
[c] Incomplete H I velocity coverage.
[d] H I tail.
[e] Closely interacting pair. Values apply for the entire system.

extending beyond the optical disk in the direction opposite of the group center (Figure 6). Neither of these objects is H I deficient, so any stripping activity must have recently commenced. Their respective radial velocities relative to the group mean of 200 and 320 km s^{-1} imply Mach numbers of $\mathcal{M} \gtrsim 0.4$ and $\gtrsim$0.6, respectively, for an ambient gas temperature of $T \approx 1$ keV. Although both galaxies are currently beyond the radius to which intragroup gas is detected ($R \approx 500$ and ≈900 kpc), their H I morphologies are suggestive of ongoing ram pressure (or viscous) stripping. Multi-wavelength observations and higher-resolution H I data would be required to confirm this (e.g., Murphy et al. 2009). Another relatively isolated spiral, IC 2293 at $R \sim 470$ kpc, displays no H I tail but is highly deficient ($\rm Def_{H\,I} = 0.55$), and is also a candidate for recent ram pressure stripping.

To test for the *global* importance of ram pressure stripping within the group, we next consider the radial distribution of ISM detections. To put all galaxies on an equal footing, their thermal X-ray luminosities and H I masses were normalized by the galaxy L_K. Excluding again the central galaxy NGC 2563, evidence for hot gas is seen in only five of the group members, and Figure 8 shows that all of these reside relatively far from the group center, with four out of five located beyond the radius $R \sim 400$ kpc to which intragroup gas is detected. In contrast, no hot ISM component is found within $R \sim 300$ kpc, where several of the optically luminous early types reside. This includes NGC 2562 at $R \sim 90$ kpc, the closest bright galaxy to the group center, with an upper limit to $L_{\rm X,th}$ which is an order of magnitude below the value of $\log (L_{\rm X,th}/L_K) \simeq -4.6$ suggested by the L_K–$L_{\rm X,th}$ relation for early types in groups (Jeltema et al. 2008).

To further illustrate this point, we note that, given our X-ray detection limits (Section 4.1), the Kim & Fabbiano (2004) relation would suggest that we should detect all early-type members brighter than $\log (L_K/L_\odot) \approx 10.0$, irrespective of their hot gas content. In practice, only 8/14 (57% ± 25%) are detected, even if including NGC 2563 itself and excluding Sa galaxies. The bottom panel in Figure 8 shows the cumulative fraction of group members covered by *Chandra* above this L_K that is X-ray detected, and the fraction that also contains evidence for a thermal component. While the former remains constant with R, the thermal fraction drops toward the group core. Although subject to large Poisson errors, this result is consistent with hot ISM having been stripped within the dense group core, while the more distant galaxies retaining a thermal component have yet to experience peak ram pressure during their orbit (but see also Balogh et al. 2000).

In contrast, galaxies with a detectable *cold* ISM component are distributed more evenly with R. This is illustrated in Figure 9(a), which compares our measured H I masses to those of similar galaxies in the field. A handful of galaxies show evidence of a significant shortfall in H I content (i.e., $\rm Def_{H\,I} \gtrsim 0.5$), but the values scatter broadly around $\rm Def_{H\,I} = 0$ and show no systematic dependence on R. A Kolmogorov test was performed to test whether the inferred deficiencies are, in fact, consistent with being drawn from a Gaussian parent distribution centered at $\rm Def_{H\,I} = 0$ with some width σ. We find that for σ in the range 0.3–0.5, this probability is at least 85%, regardless of whether

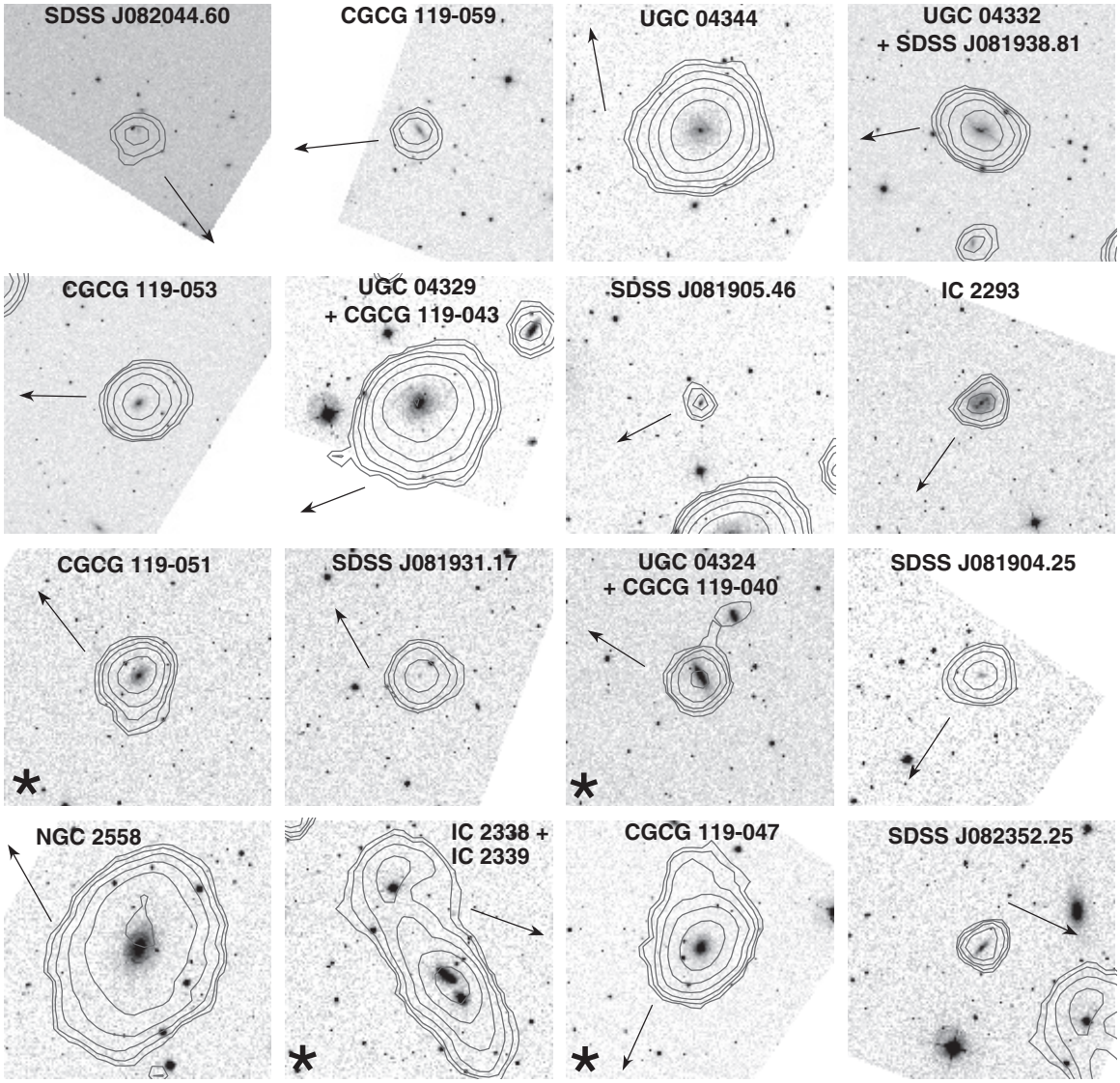

Figure 6. H I contours overlaid on SDSS *r*-band images for the 20 H I-detected group members in order of increasing distance from the group center. Each image is $7' \times 7'$ ($\sim$130 $\times$ 130 kpc), with contours at 0.04, 0.08, 0.16, 0.32, 0.64, 1.28, and 2.50 Jy beam^{-1}. Arrows indicate the direction to the group center. Objects with significant H I tails/extensions are marked with an asterisk in the lower left corner.

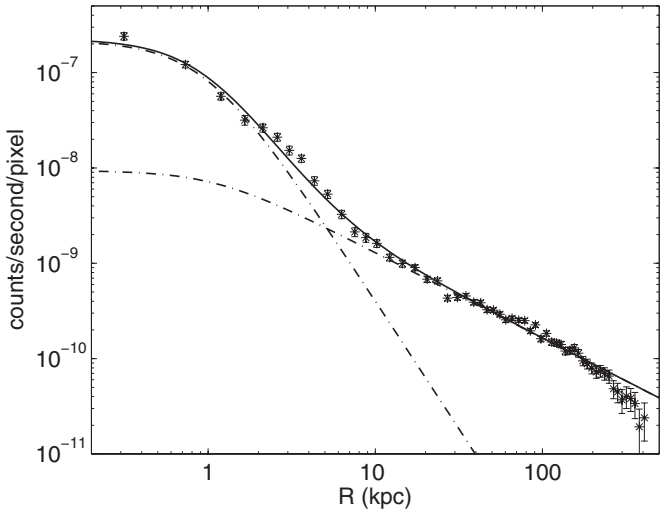

Figure 7. Background-subtracted radial profile of the 0.5–2 keV intragroup emission, extracted in 2″ pixels. The solid line shows the best-fit double β-model, with the individual model components shown as dot-dashed lines. Error bars include uncertainties on the background level.

the upper/lower limits and the highly deficient CGCG119-040 are included. There is thus no strong evidence from this that the large Sa–Sc group members are globally H I deficient. However, we present evidence in Section 5.3 that the late-type population as a whole *is* deficient relative to the field.

The estimated H I deficiencies depend on assumed galaxy morphology and the somewhat uncertain comparison values for field galaxies. A more robust measure of the relative H I content within the group members might be provided by $M_{\rm H\,I}/L_K$. The dependence of this quantity on R is shown in Figure 9(b). Note that at fixed R, lower-mass galaxies would be more easily ram pressure stripped, but they are also likely to be more H I-rich to begin with. To take this into account, the galaxies were divided into three bins of comparable L_K. Figure 9(b) confirms that even at "fixed" L_K, there is no systematic radial dependence of H I content within the group, and hence that ram pressure stripping of cold ISM is unlikely to be globally important in this system.

5.2. Evidence for Tidal Gas Stripping

The presence of H I tails associated with close galaxy pairs is commonly taken as a sign of tidal encounters (de Mello et al.

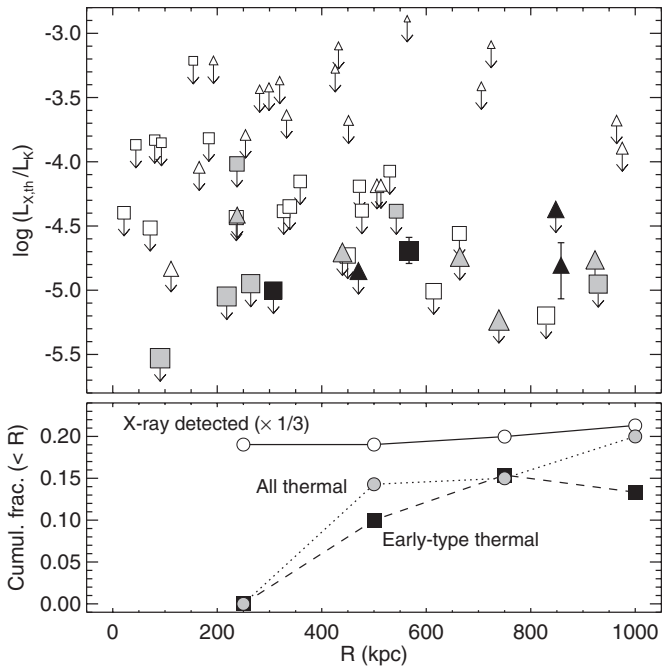

Figure 8. *K*-band-normalized thermal X-ray luminosity as a function of projected group radius *R*, excluding the central galaxy NGC 2563. Symbols are as in Figure 4, with symbol sizes scaling with galaxy L_K. The bottom panel shows the cumulative fraction of optically bright ($L_K > 10^{10}\,L_\odot$) group members within a given *R* that are X-ray detected (empty symbols; scaled down by a factor of three for ease of comparison), the fraction containing a thermal component (gray), and that of the early types doing so (black).

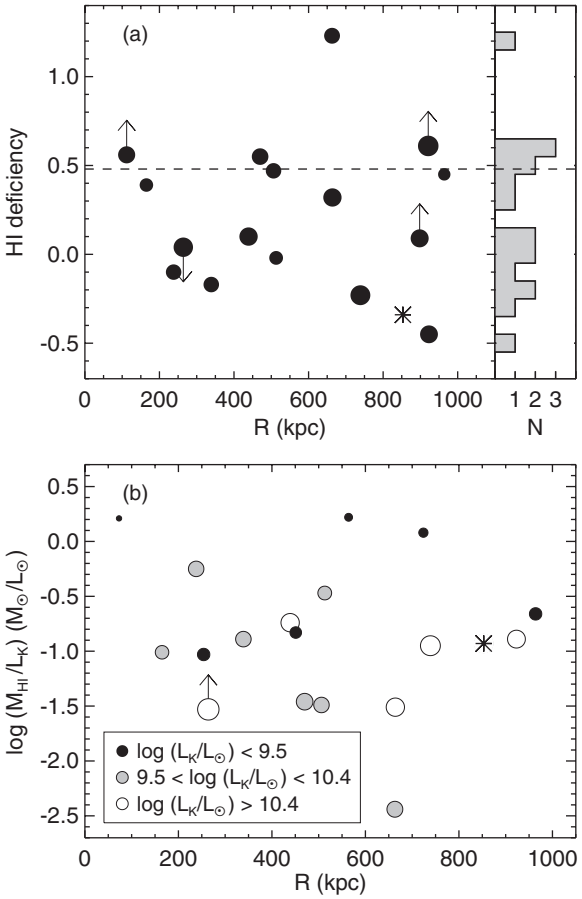

Figure 9. (a) H I deficiencies $\mathrm{Def_{H\,I}}$ of all large group spirals of types Sa through Sc, along with a histogram of $\mathrm{Def_{H\,I}}$. Galaxies above the dashed line are deficient by at least a factor of three. The upper limit represents UGC 4332, which has incomplete H I velocity coverage and so only a lower limit to its H I mass (see Table 3). (b) *K*-band-normalized H I masses for all H I-detected group members, color-coded according to galaxy L_K. The lower limit marks UGC 4332. In both plots, symbol sizes scale with L_K, and asterisk represents the IC 2338/2339 pair.

2008; Koopmann et al. 2008). NGC 2563 contains two galaxy pairs with clear H I extensions indicating such encounters. The most prominent of these is associated with IC 2338 and IC 2339, a spiral pair separated by only ∼15 kpc in projection and ∼20 km s^{-1} in velocity. The SDSS images show evidence for a stellar bridge between the galaxies, supporting a tidal origin for the H I tails. An H I extension is also connecting UGC 04324 with CGCG119-040; the latter represents the most H I deficient group member (deficient by a factor of ∼15), with all its H I associated with the H I bridge. While no corresponding stellar feature is seen in the relatively shallow SDSS images, the H I morphology is strongly suggestive of a tidal encounter.

To explore whether recent removal of cold ISM through tidal interactions can generally explain the observed H I deficiencies within the group, we show in Figure 10(a) the H I deficiencies as a function of projected distance R_1 to the nearest neighbor. If excluding the closely interacting IC 2338/2339 pair and the upper/lower limits, a Kendall correlation test suggests an anticorrelation at the 1.0σ level. Including the upper/lower limits at their nominal values strengthens the correlation significance to 2.2σ. The correlation with R_1 remains significant at the 2σ level when instead considering the normalized H I masses in Figure 10(b). While only indicative, this result is consistent with some H I having been removed in galaxy–galaxy interactions within the group.

Since strong tidal interactions require proximity of two galaxies in both position and velocity space, a plot of H I content against R_1 may be subject to large scatter due to some galaxies being close in projection only. For each galaxy, we therefore also consider the minimum value of

$$\xi = \sqrt{(\Delta R/\Delta R_{\rm max})^2 + (\Delta v_r/\Delta v_{\rm max})^2}, \qquad (2)$$

where ΔR and Δv_r are the separations in projection and radial velocity between *any* two group members, and $\Delta R_{\rm max} \approx 2.1$ Mpc and $\Delta v_{\rm max} \approx 1600$ km s^{-1} are the corresponding maximum values between all galaxies in NGC 2563. Strong interactions would require $\xi \ll 1$, and, if generally prominent in removing H I, would imply a correlation between H I content and ξ for small values of the latter. For NGC 2563, one might expect interactions to be important up to at least $\xi \approx 0.1$, as this would correspond to two galaxies at the same v_r separated by $\Delta R \lesssim 200$ kpc, or to a physically "overlapping" pair with $\Delta v \lesssim 160$ km s^{-1}. As suggested by Figures 10(c) and (d), there is some evidence of such a correlation for $\xi \lesssim 0.1$ among the individually H I-detected galaxies. However, this is significant at less than 2σ, so we can only conclude that our results are at least consistent with some H I removal due to galaxy–galaxy interactions. Repeating this analysis for the X-ray-detected group members reveals no indication of a systematic trend in $L_{\rm X,th}/L_K$ with either R_1 or ξ. However, many of these galaxies have X-ray luminosities only slightly above our completeness limit, so deeper observations of a larger sample would be required to confirm this result within groups in general.

5.3. Global H I Properties of the Group

Our comprehensive VLA coverage of NGC 2563 enables a census of the global amount and distribution of H I in the group,

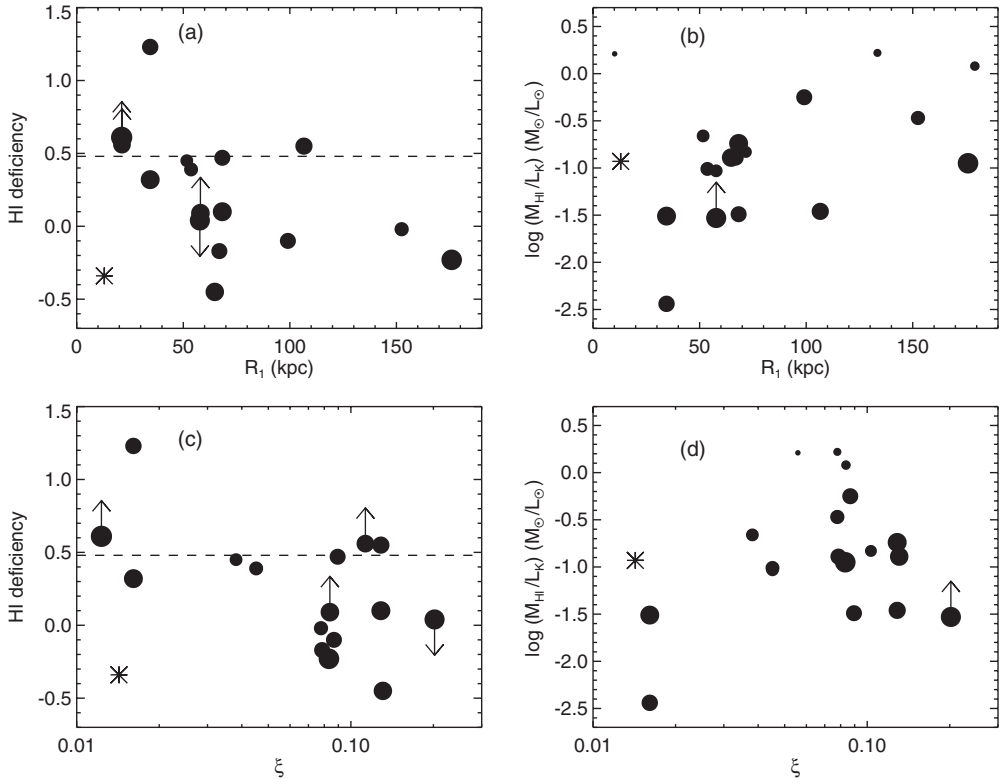

Figure 10. (a) H I deficiencies $\mathrm{Def_{H\,I}}$ of all large group spirals of types Sa through Sc as a function of projected distance R_1 to the nearest neighbor. The dashed line is as in Figure 9. (b) K-band-normalized H I masses for the H I-detected objects against R_1. The lower limit marks UGC 4332. (c) Same as (a), but as a function of ξ from Equation (2). (d) Same as (b), but as a function of ξ. In all plots, symbol sizes scale with L_K, and asterisk represents the IC 2338/2339 pair.

and provides further evidence of recent H I mass loss from the group members. Based on measurements from the H I Parkes All Sky Survey, Evoli et al. (2011) have quantified the typical H I mass for late-type galaxies (Sb and later) in the general "field" with $M_* > 10^8\,M_\odot$:

$$M_{\mathrm{H\,I}} = M_1 \left(\frac{M_*}{M_2}\right)^{0.19} \left[1 + \left(\frac{M_*}{M_2}\right)^{0.76}\right], \qquad (3)$$

where $M_1 = 3.36 \times 10^9\,M_\odot$ and $M_2 = 3.3 \times 10^{10}\,M_\odot$. To compare this to results for NGC 2563, we used estimates of M_* for the group members from SDSS,[16] available for all but six of the 64 members; for those six, we assume a K-band stellar mass-to-light ratio of 0.55, which is the average for the members with both L_K and M_* available. Equation (3) would then suggest a total H I mass of the relevant group members of $6.7 \pm 2.0 \times 10^{10}\,M_\odot$, whereas the value inferred from Table 3 is $M_{\mathrm{H\,I}} < 4.4 \times 10^{10}\,M_\odot$, when including the average 3σ upper limit of $2 \times 10^8\,M_\odot$ for the undetected members. This suggests that globally the $M_* > 10^8\,M_\odot$ late types in the group have suffered mild H I mass loss with respect to similar field galaxies. Compared to estimates of $\mathrm{Def_{H\,I}}$, this result may represent a more robust estimate of global H I deficiency within the group, as it also includes smaller galaxies, depends less sensitively on the inferred morphology and optical size of individual group members, and takes the dispersion seen for field galaxies into account.

We also derive a total stellar mass in the group of $M_* \approx 1.1 \times 10^{12}\,M_\odot$ for all the 64 spectroscopically identified members, and a corresponding total range of $M_{\mathrm{H\,I}} = (5.7\text{–}6.5) \times 10^{10}\,M_\odot$. This implies $M_{\mathrm{H\,I}}/M_* = 0.054\text{–}0.062$ for the full group (down to our 98% spectroscopic completeness limit of $M_r = -17$), under the plausible assumption that our VLA observations are not missing any large-scale diffuse H I. Future comparison of this result for an X-ray bright group to other groups and clusters could provide further information on the nature of gas removal in these environments.

On the largest scales, the distribution of H I-detected galaxies in Figure 5 reveals a peculiar lopsidedness, with 16 of the 20 detections occurring on the western side of the group. This is not simply due to asymmetric spatial VLA coverage, as demonstrated in Figure 1, nor due to a larger fraction of H I deficient galaxies in the east. The wide velocity coverage of our VLA data ($\Delta v_r \approx \pm 3\sigma_{\mathrm{biwt}}$) further renders it unlikely that a significant fraction of potential group members have been missed on the eastern side of the system. The lopsided H I distribution thus reflects a real asymmetry in the distribution of late-type members, with nearly all the large spirals located in the western half of the group.

The origin of this asymmetry remains unclear. One possibility is that the western spirals are part of an infalling subgroup, but echoing an earlier conclusion by Zabludoff & Mulchaey (1998b), we find no evidence for kinematic substructure in the group using the technique pioneered by Dressler & Shectman (1988). Another possible scenario is that galaxy morphologies have been modified by strong interactions with a similarly asymmetric intragroup medium. This can be ruled out, however, because the intragroup gas distribution in NGC 2563 appears fairly symmetric on large scales and, if anything, seems more strongly extended to the west (see Figure 2 and Mulchaey & Zabludoff 1998). Finally, exploiting the extensive SDSS coverage in this field, we have also examined the overall galaxy

[16] http://www.mpa-garching.mpg.de/SDSS/DR7/

distribution within a projected distance of $R = 5$ Mpc of the group center, and find no evidence for a general large-scale enhancement in galaxy density on the western side of the group. Further studies of other groups on very large scales may help establish how common such morphological segregations are in these systems.

6. SUMMARY AND CONCLUSIONS

Our extensive *Chandra* and VLA coverage of the NGC 2563 galaxy group has enabled us to probe both the hot and cold ISM within a nearby group out to ∼1.4 times the estimated virial radius. The main aim has been to characterize the evidence for galactic gas removal in this system and understand the mechanisms involved. Although the limited number of galaxies preclude strong conclusions based on a single group, our results suggest that both hot and cold gas have been stripped from some of the group members, and that both ram pressure stripping and gas removal via galaxy–galaxy interactions are all occurring simultaneously within this one system. This is based on the following evidence.

1. The thermal X-ray deficiency of optically luminous early-type galaxies in the group core suggests recent ram pressure stripping of their hot gas. The central group galaxy aside, no hot ISM is detected within $R \sim 300$ kpc from the group core, whereas four out of the five non-central galaxies with such a component reside beyond the radius to which intragroup gas is detected. The thermal luminosity of the bright early type closest to the group core (NGC 2562) is at least an order of magnitude below that expected for typical group galaxies of the relevant L_K (Jeltema et al. 2008).
2. Comparison of the H I content of the late-type group members to that of similar galaxies in the field suggests that the former are, on average, mildly deficient in H I. This points to one or more mechanisms removing cold ISM within the group.
3. Ram pressure (or viscous) stripping of cold gas is suspected in a few cases. The H I data reveal one relatively isolated spiral (IC 2293) which is H I deficient by more than a factor of three. Another two such spirals show H I morphologies suggestive of an ongoing ram pressure interaction, with H I tails pointing away from the group core (CGCG 119-047 and 119-051 in Figure 6). However, these are not (yet) H I deficient by the usual definition, indicating that significant interactions with the intragroup medium may have only recently commenced.
4. Ongoing galaxy–galaxy interactions removing H I are also strongly suggested in at least two cases. The two most prominent H I tails/extensions in the group occur within close galaxy pairs, and the most H I deficient group member (CGCG 119-040, deficient by a factor of ∼15) is a member of one of these. Suggestive evidence is further seen for galaxies with close neighbors in position–velocity space to show relatively low H I content, consistent with tidal stripping of H I.

The inference that ram pressure stripping of hot galactic gas may have occurred in the central group regions would be in line with other *Chandra* studies of group and cluster galaxies (Rasmussen et al. 2006; Sun et al. 2007), and with simulations which suggest that such stripping can be efficient even in small galaxy groups (Kawata & Mulchaey 2008). However, it is worth noting that a large fraction of early-type galaxies generally do retain halos even in X-ray bright groups, including some in NGC 2563, and that such halos are not generally underluminous compared to those of galaxies in the field (Jeltema et al. 2008; Mulchaey & Jeltema 2010). Despite the detection of a hot intragroup medium within NGC 2563 out to $R \approx R_{500}$, there is also no global evidence for ram pressure stripping of the *cold* ISM within the group. Specifically, no radial trends are seen in the stellar-mass-normalized H I content among the 20 H I-detected group members.

The indicative result that ram pressure may affect only the hot ISM in typical group galaxies is consistent with existing numerical studies (Kawata & Mulchaey 2008; Rasmussen et al. 2008). Galaxy–galaxy interactions remain the main candidate for removing cold ISM within NGC 2563 and explaining the global H I deficiency inferred for the late-type group members. Other studies have also implied that tidal encounters have an important impact on the H I properties of galaxies in groups (Kern et al. 2008; Rasmussen et al. 2008). In addition, such encounters may work to enhance the susceptibility of a galaxy to ram pressure stripping by perturbing the distribution of the cold gas (Davis et al. 1997; Mayer et al. 2006). Nevertheless, despite the detection of two new group members from our optically blind H I search, we find no evidence within the NGC 2563 group for isolated, optically dark H I clouds that might represent previously removed material.

Given the small number of luminous galaxies in a single group, similar studies of a larger group sample will be required to better understand how the group environment impacts galaxy evolution. For example, we note that the inferred H I-to-stellar mass ratio of ≈0.06 inferred for this X-ray bright group may provide a useful benchmark for the H I content of dynamically evolved groups. Future comparison of this result to those of X-ray faint systems, richer clusters, and groups at higher redshift (of which the upcoming Square Kilometre Array should detect many thousands) could further improve our understanding of the nature and epoch of gas removal in dense environments. Such studies would also help to address the commonality of the highly lopsided distribution of H I seen in NGC 2563, which reflects a puzzling galaxy morphological segregation within the group.

We are grateful to the referee for a careful and constructive report which significantly improved the presentation of our results. We thank Christy Tremonti for providing the emission-line ratios for the SDSS spectra. This research has made use of the NASA/IPAC Extragalactic Database (NED). J.R. acknowledges support by the Carlsberg Foundation. X.B. thanks Professor Zhang, S. Nan, and R. Fengyun from Tsinghua Center for Astrophysics (THCA) for discussions on *Chandra* analysis. Support for this work was provided by the National Science Foundation under grant number 0607643 to Columbia University, and by the National Aeronautics and Space Administration through Chandra Award Number G07-8134X issued by the Chandra X-ray Observatory Center, which is operated by the Smithsonian Astrophysical Observatory for and on behalf of the National Aeronautics Space Administration under contract NAS8-03060.

REFERENCES

Arnaud, K. A. 1996, in ASP Conf. Ser. 101, Astronomical Data Analysis Software and Systems V, ed. G. H. Jacoby & J. Barnes (San Francisco, CA: ASP), 17
Bailin, J., & Ford, A. 2007, MNRAS, 375, L41
Baldry, I. K., Balogh, M. L., Bower, R. G., et al. 2006, MNRAS, 373, 469

Baldwin, J. A., Phillips, M. M., & Terlevich, R. 1981, PASP, 93, 5
Balogh, M. L., Navarro, J. F., & Morris, S. L. 2000, ApJ, 540, 113
Barnes, J. E. 1989, Nature, 338, 123
Beers, T. C., Flynn, K., & Gebhardt, K. 1990, AJ, 100, 32
Bureau, M., & Carignan, C. 2002, AJ, 123, 1316
Burstein, D., Krumm, N., & Salpeter, E. E. 1987, AJ, 94, 883
Cash, W. 1979, ApJ, 228, 939
Cayatte, V., Kotanyi, C., Balkowski, C., & van Gorkom, J. H. 1994, AJ, 107, 1003
Chamaraux, P., Balkowski, C., & Gerard, E. 1980, A&A, 83, 38
Chung, A., van Gorkom, J. H., Kenney, J. D. P., Crowl, H., & Vollmer, B. 2009, AJ, 138, 1741
Chung, A., van Gorkom, J. H., Kenney, J. D. P., & Vollmer, B. 2007, ApJ, 659, L115
Cortese, L., Catinella, B., Boissier, S., Boselli, A., & Heinis, S. 2011, MNRAS, 415, 1797
Crowl, H. H., Kenney, J. D. P., van Gorkom, J. H., & Vollmer, B. 2005, AJ, 130, 65
Cucciati, O., Iovino, A., Kovač, K., et al. 2010, A&A, 524, A2
Davis, D. S., Keel, W. C., Mulchaey, J. S., & Henning, P. A. 1997, AJ, 114, 613
de Mello, D. F., Smith, L. J., Sabbi, E., et al. 2008, AJ, 135, 548
di Serego Alighieri, S., Gavazzi, G., Giovanardi, C., et al. 2007, A&A, 474, 851
Dressler, A., & Shectman, S. A. 1988, AJ, 95, 985
Evoli, C., Salucci, P., Lapi, A., & Danese, L. 2011, ApJ, 743, 45
Fabbiano, G. 2006, ARA&A, 44, 323
Fabbiano, G., Kim, D.-W., & Trinchieri, G. 1992, ApJS, 80, 531
Finoguenov, A., Ponman, T. J., Osmond, J. P. F., & Zimer, M. 2007, MNRAS, 374, 737
Gastaldello, F., Buote, D. A., Humphrey, P. J., et al. 2007, ApJ, 669, 158
Gehrels, N. 1986, ApJ, 303, 336
Jeltema, T. E., Binder, B., & Mulchaey, J. S. 2008, ApJ, 679, 1162
Kalberla, P. M. W., Burton, W. B., Hartmann, D., et al. 2005, A&A, 440, 775
Kantharia, N. G., Ananthakrishnan, S., Nityananda, R., & Hota, A. 2005, A&A, 435, 483
Kauffmann, G., Heckman, T. M., Tremonti, C., et al. 2003a, MNRAS, 346, 1055
Kauffmann, G., Heckman, T. M., White, S. D. M., et al. 2003b, MNRAS, 341, 54
Kauffmann, G., White, S. D. M., Heckman, T. M., et al. 2004, MNRAS, 353, 713
Kawata, D., & Mulchaey, J. S. 2008, ApJ, 672, L103
Kenney, J. D. P., van Gorkom, J. H., & Vollmer, B. 2004, AJ, 127, 3361
Kern, K. M., Kilborn, V. A., Forbes, D. A., & Koribalski, B. 2008, MNRAS, 384, 305
Kewley, L. J., Dopita, M. A., Sutherland, R. S., Heisler, C. A., & Trevena, J. 2001, ApJ, 556, 121
Kilborn, V. A., Forbes, D. A., Barnes, D. G., et al. 2009, MNRAS, 400, 1962
Kilborn, V. A., Forbes, D. A., Koribalski, B. S., Brough, S., & Kern, K. 2006, MNRAS, 371, 739
Kim, D.-W., & Fabbiano, G. 2004, ApJ, 611, 846
Koopmann, R. A., Giovanelli, R., Haynes, M. P., et al. 2008, ApJ, 682, L85
Levy, L., Rose, J. A., van Gorkom, J. H., & Chaboyer, B. 2007, AJ, 133, 1104
Liedahl, D. A., Osterheld, A. L., & Goldstein, W. H. 1995, ApJ, 438, L115
Mamon, G. A. 2007, in ESO Symp., Groups of Galaxies in the Nearby Universe, ed. I. Saviane, V. Ivanov, & J. Borissova (Berlin: Springer), 203
Mayer, L., Mastropietro, C., Wadsley, J., Stadel, J., & Moore, B. 2006, MNRAS, 369, 1021
McConnachie, A. W., Venn, K. A., Irwin, M. J., Young, L. M., & Geehan, J. J. 2007, ApJ, 671, L33
Mewe, R., Gronenschild, E. H. B. M., & van den Oord, G. H. J. 1985, A&AS, 62, 197
Mihos, J. C., & Hernquist, L. 1996, ApJ, 464, 641
Miller, M. C., & Colbert, E. J. M. 2004, Int. J. Mod. Phys. D, 13, 1
Montero-Dorta, A. D., & Prada, F. 2009, MNRAS, 399, 1106
Moore, B., Lake, G., Quinn, T., & Stadel, J. 1999, MNRAS, 304, 465
Morganti, R., de Zeeuw, P. T., Oosterloo, T. A., et al. 2006, MNRAS, 371, 157
Mulchaey, J. S., Davis, D. S., Mushotzky, R. F., & Burstein, D. 2003, ApJS, 145, 39
Mulchaey, J. S., & Jeltema, T. E. 2010, ApJ, 715, L1
Mulchaey, J. S., & Zabludoff, A. I. 1998, ApJ, 496, 73
Murphy, E. J., Kenney, J. D. P., Helou, G., Chung, A., & Howell, J. H. 2009, ApJ, 694, 1435
Navarro, J. F., Frenk, C. S., & White, S. D. M. 1997, ApJ, 490, 493
Nilson, P. 1973, Acta Universitatis Upsaliensis. Nova Acta Regiae Societatis Scientiarum Upsaliensis—Uppsala Astronomiska Observatoriums Annaler (Uppsala: Astronomiska Observatorium)
Nulsen, P. E. J. 1982, MNRAS, 198, 1007
Osmond, J. P. F., & Ponman, T. J. 2004, MNRAS, 350, 1511
O'Sullivan, E., Forbes, D. A., & Ponman, T. J. 2001, MNRAS, 328, 461
O'Sullivan, E., Ponman, T. J., & Collins, R. S. 2003, MNRAS, 340, 1375
Peng, Y.-j., Lilly, S. J., Kovač, K., et al. 2010, ApJ, 721, 193
Quilis, V., Moore, B., & Bower, R. 2000, Science, 288, 1617
Rasmussen, J., Ponman, T. J., & Mulchaey, J. S. 2006, MNRAS, 370, 453
Rasmussen, J., Ponman, T. J., Verdes-Montenegro, L., Yun, M. S., & Borthakur, S. 2008, MNRAS, 388, 1245
Rasmussen, J., Sommer-Larsen, J., Pedersen, K., et al. 2009, ApJ, 697, 79
Read, A. M., & Ponman, T. J. 2001, MNRAS, 328, 127
Roberts, T. P. 2007, Ap&SS, 311, 203
Schröder, A., Drinkwater, M. J., & Richter, O.-G. 2001, A&A, 376, 98
Sengupta, C., Balasubramanyam, R., & Dwarakanath, K. S. 2007, MNRAS, 378, 137
Solanes, J. M., Giovanelli, R., & Haynes, M. P. 1996, ApJ, 461, 609
Solanes, J. M., Manrique, A., García-Gómez, C., et al. 2001, ApJ, 548, 97
Sun, M., Jones, C., Forman, W., et al. 2007, ApJ, 657, 197
Sun, M., Voit, G. M., Donahue, M., et al. 2009, ApJ, 693, 1142
Tremonti, C. A., Heckman, T. M., Kauffmann, G., et al. 2004, ApJ, 613, 898
Tüllmann, R., Breitschwerdt, D., Rossa, J., Pietsch, W., & Dettmar, R.-J. 2006, A&A, 457, 779
Verdes-Montenegro, L., Yun, M. S., Williams, B. A., et al. 2001, A&A, 377, 812
Vikhlinin, A., Kravtsov, A., Forman, W., et al. 2006, ApJ, 640, 691
Zabludoff, A. I., & Mulchaey, J. S. 1998a, ApJ, 496, 39
Zabludoff, A. I., & Mulchaey, J. S. 1998b, ApJ, 498, L5
Zabludoff, A. I., & Mulchaey, J. S. 2000, ApJ, 539, 136